EUROPHYSICS LETTERS 1 September 2001

Europhys. Lett., **55** (5), pp. 746–752 (2001)

Hysteresis and bistability in a realistic model for IP_3-driven Ca^{2+} oscillations

J. J. Torres[1](*), P. H. G. M. Willems[2], H. J. Kappen[1] and W. J. H. Koopman[2]

[1] *Department of Medical Physics and Biophysics, University of Nijmegen Geert Grooteplein 21, 6525 EZ Nijmegen, The Netherlands*

[2] *Departments of Biochemistry and Cell Physiology, University of Nijmegen Geert Grooteplein Zuid 30, 6525 AD Nijmegen, The Netherlands*

(received 17 November 2000; accepted in final form 13 June 2001)

PACS. 87.10.+e – General theory and mathematical aspects.
PACS. 87.16.-b – Subcellular structure and processes.
PACS. 87.16.Ac – Theory and modeling; computer simulation.

Abstract. – We present a new model for inositol triphosphate (IP_3)-induced cytosolic Ca^{2+} oscillations in non-excitable cells. The model includes the various Ca^{2+} in- and efflux pathways reported to exist in these cells. In particular, it features the complex regulation of the Ca^{2+} release from the endoplasmic reticulum (ER) by IP_3, cytosolic Ca^{2+} and Ca^{2+} in the ER. Bifurcation analysis revealed that the model accurately predicts the cytosolic Ca^{2+} dynamics in a typical non-excitable cell. Diffusional coupling of this model in a two-dimensional network shows hysteresis and bistability in its collective dynamics. Depending on the strength of the diffusion constant, we find traveling or spiral waves as solutions of this system.

Ionized calcium (Ca^{2+}) not only represents the most common signal transduction element relaying information within cells to control a wide array of activities including secretion, contraction and cell proliferation, but also is invariably involved in cell death [1]. To coordinate all of these functions, cytosolic Ca^{2+} ($[Ca^{2+}]_c$) needs to be precisely regulated in space, time and amplitude. Normal $[Ca^{2+}]_c$ at 100 nM is 20000 fold lower than the 2 mM concentration found extracellularly (fig. 1). Under resting conditions this gradient is maintained by active extrusion of cytosolic Ca^{2+} by Ca^{2+} ATPases present in the plasma membrane (PMCA) and the sarco- or endoplasmic reticulum (SERCA). These pumps counterbalance the leak of Ca^{2+} into the cytosol from both the extracellular space ($leak_{PM}$) and the endoplasmic reticulum Ca^{2+} store ($leak_{ER}$).

A wide variety of extracellular stimuli cause the increase of $[Ca^{2+}]_c$ to exert their effect. In non-excitable cells, this increase is triggered by inositol(1,4,5)-triphosphate (IP_3), produced upon activation of phospholipase C (PLC) [1]. IP_3 rapidly diffuses into the cytosol, where it interacts with an ER Ca^{2+} channel (the IP_3R) to promote the release of Ca^{2+}. Depending on the cell type, the resulting cytosolic Ca^{2+} signal can have a complex spatio-temporal composition [1]. It is generally recognized that, in the presence of a constant external stimulus, the $[Ca^{2+}]_c$ displays periodic spiking behavior (fig. 2A). These Ca^{2+} oscillations can be spatially localized or extended, spreading as a wave throughout the entire cell. Forward propagation of

(*) Present address: Departamento de Electromagnetismo y Física de la Materia, University of Granada - E-18071 Granada, Spain. E-mail: jtorres@onsager.ugr.es

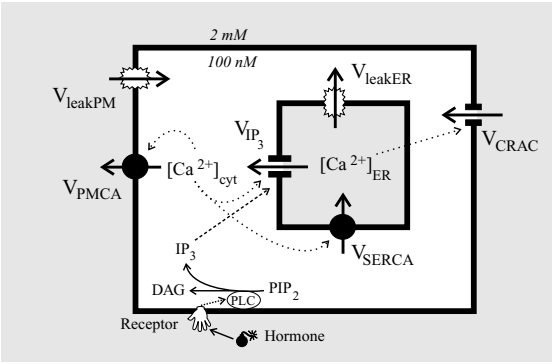

Fig. 1 – Schematic representation of the Ca^{2+} fluxes present in the model and the diverse regulatory interactions of Ca^{2+} (dotted lines). (See text for explanation.) Grey background: compartments with high [Ca^{2+}], white background: compartments with low [Ca^{2+}].

such Ca^{2+} waves is postulated to be driven by a sequence of Ca^{2+} diffusion and Ca^{2+}-induced Ca^{2+} release (CICR) from ER Ca^{2+} stores. Ca^{2+} release is terminated by closure of Ca^{2+} channels, after which Ca^{2+} is removed from the cytosol by the combined action of the PMCA and SERCA. A Ca^{2+} influx pathway in the plasma membrane, generally referred to as Ca^{2+} release-activated Ca^{2+} channel (CRAC), is activated to compensate for the loss of Ca^{2+} via the PMCA [2]. Here, we present a new mathematical model describing the temporal aspects of cytosolic Ca^{2+} signaling in non-excitable cells. The model incorporates a full description

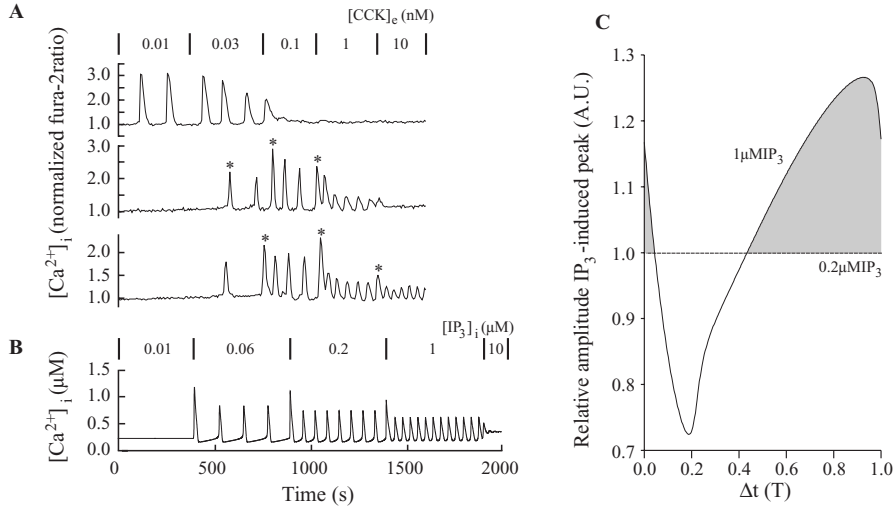

Fig. 2 – A) Cytosolic Ca^{2+} oscillations in pancreatic acinar cells at increasing concentrations of CCK, displaying different sensitivity to CCK. B) Ca^{2+} oscillations generated by the model, for increasing values of [IP_3]. C) Amplitude of the first Ca^{2+} spike after increasing [IP_3] from 0.2 to 1 μM as a function of Δt (see text for details). The y-axis scale is relative to the amplitude of the ongoing oscillation (horizontal line). Parameter values were: $V^{\max}_{IP_3} = 617.5\ \mu M/\min$, $V^{\max}_{CRAC} = 0.51\ \mu M^2/\min$, $V^{\max}_{SERCA} = 62.1\ \mu M/\min$, $V^{\max}_{PMCA} = 8.5\ \min^{-1}$, $\mu_0 = 0.125$, $\mu_1 = 1 - \mu_0$, $\tau_h = 2\,\min$, $K_R = 1.3\ \mu M$, $K_A = 0.5\ \mu M$, $K_h = 1\ \mu M$, $K_{SERCA} = 0.74\ \mu M$, $k_{CRAC} = 0.05\ \mu M$, $k_{PM} = 0.0017\ \min^{-1}$, $k_{ER} = 1.3\ \min^{-1}$ and $K_{IP_3} = 0.5\ \mu M$.

of the Ca^{2+} fluxes mentioned above and features the combined regulation of the IP_3R by IP_3, $[Ca^{2+}]_c$ and Ca^{2+} inside the ER.

Mathematically, the model consists of two compartments with a variable free $[Ca^{2+}]$, namely the cytosol, c, and the ER, c_{ER}. The dynamic changes of c and c_{ER} are governed by the equations

$$\frac{dc}{dt} = V_{IP_3} + V_{leak_{ER}} + V_{leak_{PM}} + V_{CRAC} - V_{SERCA} - V_{PMCA}, \quad (1)$$

$$\frac{dc_{ER}}{dt} = V_{SERCA} - V_{IP_3} - V_{leak_{ER}}, \quad (2)$$

where the rate of IP_3-mediated Ca^{2+} release from the ER is modeled as

$$V_{IP_3} = V_{IP_3}^{max} \cdot \left(\mu_0 + \frac{\mu_1[IP_3]}{[IP_3] + K_{IP_3}}\right) \cdot \frac{c_{ER}^2}{c_{ER}^2 + K_R^2} \cdot \frac{c^4}{c^4 + K_A^4} \cdot h\,. \quad (3)$$

In this description, we assume that the binding and dissociation of Ca^{2+} and IP_3 are in fast equilibrium. Experimental evidence shows that i) the equilibrium flux of Ca^{2+} ions through the ER Ca^{2+} channel is a sigmoidal function of $[IP_3]$ [3] (first term), ii) the open equilibrium probability of the channel is increased by c_{ER} [4] (second term) and intermediate c [4,5] (third term), and iii) the channel is deactivated by high c [5] (fourth term). The rate of deactivation, h, is modeled using first-order kinetics,

$$\frac{dh}{dt} = \frac{1}{\tau_h} \cdot \left(\frac{K_h^2}{K_h^2 + c^2} - h\right), \quad (4)$$

with time constant τ_h [6].

In our simulations, extracellular $[Ca^{2+}]$ (c_{ext}) is constant (1000 μM) and $leak_{PM}$ and $leak_{ER}$ are both assumed to be proportional to the Ca^{2+} gradient: $V_{leak_{PM}} = k_{PM} \cdot (c_{ext} - c)$ and $V_{leak_{ER}} = k_{ER} \cdot (c_{ER} - c)$, respectively. Experimental data provided by Hofer [7] show that V_{CRAC} is inversely proportional to c_{ER} and given by $V_{CRAC} = V_{CRAC}^{max} \cdot (c_{ER} - k_{CRAC})^{-1}$. The rate of SERCA pumping is cooperatively dependent on c [4] and described by $V_{SERCA} = V_{SERCA}^{max} \cdot \frac{c^2}{c^2 + K_{SERCA}^2}$. Excess Ca^{2+} is extruded into the extracellular space by the PMCA, which we assume to be linearly dependent on c: $V_{PMCA} = V_{PMCA}^{max} \cdot c$.

To validate the model we compared its output with experimental data from a typical non-excitable cell, *i.e.* the pancreatic acinar cell. This cell has been used extensively as a biological model for studying the relationship between cytosolic Ca^{2+} dynamics and cellular activities like fluid and protein secretion [8]. Using fura-2 we monitored cytosolic $[Ca^{2+}]_c$ levels in single cells during application of stepwise increasing concentrations of the peptide hormone cholecystokinin (CCK) [9]. Three typical recordings of CCK-induced $[Ca^{2+}]_c$ oscillations are depicted in fig. 2A. Figure 2B shows that the model behaves similarly upon stepwise increasing of $[IP_3]$ (cf. caption of this figure for parameter values used in the simulations).

In several experimental recordings the first Ca^{2+} spike after a stepwise increase in CCK displayed a higher amplitude (marked by asterisks in fig. 2A). This phenomenon was reproduced by our model. Figure 2C shows that the amplitude of this spike depends critically on the time interval (Δt) between the $[IP_3]$ step and the top of the preceding Ca^{2+} spike. Δt is expressed as a fraction of the spike interval T before changing $[IP_3]$. Our model predicts that elevation of $[IP_3]$ at the top of an ongoing Ca^{2+} spike (Δt is zero) further increases the amplitude of this spike. This is caused by additional release of Ca^{2+} from the ER. When Δt increases, this release is visible as a shoulder on the downstroke of the ongoing spike. A discrete first spike becomes visible after termination of the ongoing spike. This spike has a low amplitude which gradually increases with c_{ER}. When the ER is filled to a certain extent, the

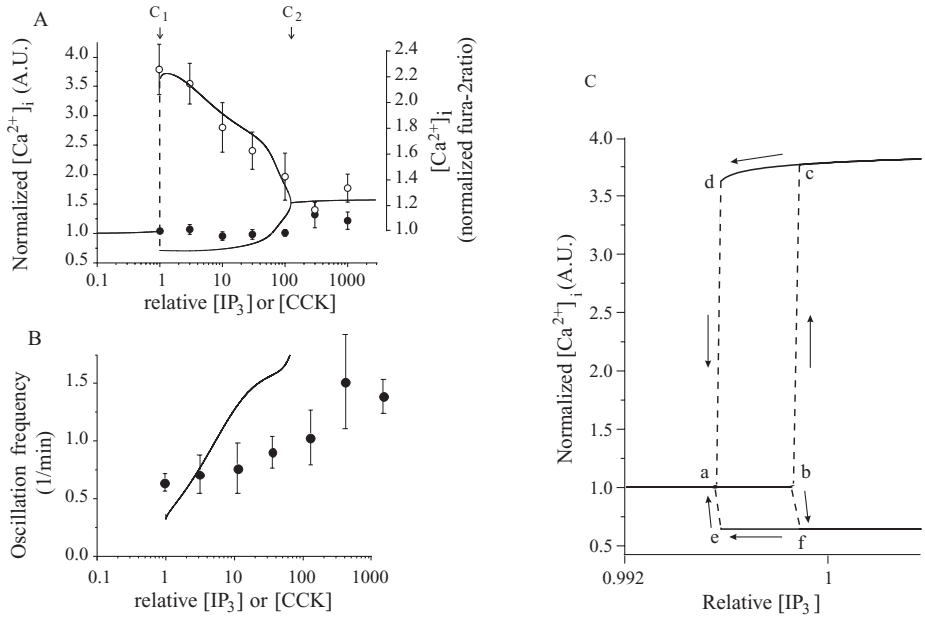

Fig. 3 – A) Bifurcation diagram for Ca^{2+} oscillations obtained from pancreatic acinar cells (data points) and the model (solid curves). B) Frequency of the Ca^{2+} oscillations in pancreatic acinar cells (points) as a function of [CCK]. The solid curve represents the theoretical frequency as a function of $[IP_3]$. C) Magnification of the theoretical bifurcation diagram near the "subcritical" Hopf bifurcation showing hysteresis (loop *abcda* or $abfea$) and bistability in the model (for parameter values, see fig. 2).

amplitude of the first Ca^{2+} spike will be higher than that of the ongoing spikes (fig. 2C; shaded area). For $\Delta t \approx T$, we are elevating IP_3 when $dc/dt \approx 0$, that is all fluxes in (1) are near to cancel. Therefore, a sudden change of IP_3 cannot induce an additional increase of c because of the low level of c_{ER} and the rapid removal of Ca^{2+} by negative fluxes (V_{SERCA} and V_{PMCA}).

To assess the quantitative performance of the model, we compared its $[IP_3]$-dependent bifurcation and frequency characteristics with that of living cells (fig. 3). A direct comparison between modeling and experimental results was not possible since individual cells displayed different sensitivities to CCK (fig. 2A). Therefore, the [CCK] at which Ca^{2+} oscillations first appeared was set to 1, thereby rescaling the CCK axis. Each subsequent [CCK] was then divided by this initial [CCK] resulting in relative [CCK]. For the model, the $[IP_3]$ was rescaled in the same way. Points in fig. 3A represent the maximum and minimum values of $[Ca^{2+}]_c$ (in normalized fura-2 ratio units) after the bifurcation point (relative [CCK] = 1). Figure 3B shows the dependency of the frequency of the Ca^{2+} oscillations as a function of the relative [CCK]. Output of the model (continuous lines in fig. 3A and B) related well with experimental results in reproducing the main features of the experimental bifurcation diagram and frequency behavior. Thus, for low values of $[IP_3]$ the model displays a sharp subcritical Hopf bifurcation, which is characterized by an abrupt appearance of high-amplitude oscillations at relative $[IP_3] = c_1$ (the two branches of the bifurcation diagram were obtained by plotting the maximum and minimum values of $[Ca^{2+}]_c$ in relative units for these oscillations). Near this bifurcation point the system exhibits hysteresis and bistability, which was revealed by slowly increasing and successively decreasing the relative $[IP_3]$ resulting in the hysteresis loop (*abcda* or $abfea$) in fig. 3C. Oscillations end at high $[IP_3]$ in a smooth supercritical Hopf bifurcation at relative $[IP_3] = c_2$

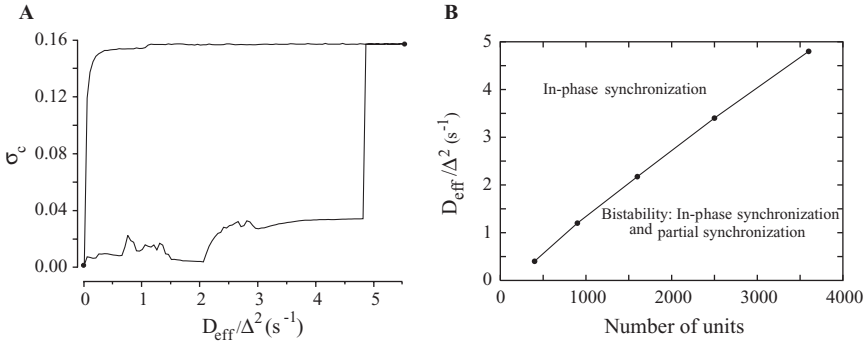

Fig. 4 – A) Variance of the collective oscillations for increasing (lower branch) and decreasing (upper branch) values of $D_{\rm eff}/\Delta^2$ (s^{-1}) in a network with 60×60 units. Hysteresis and bistability are present in the system. B) Bifurcation diagram corresponding to the collective dynamics of the whole network, showing the regions in which different synchronization regimes appear. For fixed $D_{\rm eff}$ and Δ, an increment of the size of the simulated medium (via increasing N) induced a phase transition. In pannels A and B, $[IP_3] = 0.5\ \mu$M and $K_{IP_3}(\boldsymbol{x}) = (0.65 \pm 0.05)\ \mu$M. (For other parameters, see fig. 2.)

that is preceded by a continuous decrease in oscillation amplitude with increasing $[IP_3]$.

Mathematically, our model extends the classic model of Goldbeter [4] with realistic descriptions for the rapid activation by IP_3 [3] and deactivation by c [6, 10, 11]. In contrast to other models [12] our model explicitly considers $c_{\rm ER}$. This allowed inclusion of $\text{leak}_{\rm ER}$ [8] and the stimulatory effects of $c_{\rm ER}$ on the IP_3R [13,14] and CRAC channel [2]. In our model, several parameter values differed from those described in other papers [4, 6, 15]. Especially, the maximum values of some fluxes ($V^{\rm max}_{IP_3}$, $V^{\rm max}_{\rm SERCA}$ and $V^{\rm max}_{\rm PMCA}$) had to be about 60 times smaller for reproducing the temporal scale of the $[Ca^{2+}]_c$ oscillations recorded in the experiments. This might reflect low overall PMCA/SERCA pump densities [16], low expression levels of (different subtypes of) the IP_3R and/or the presence of IP_3R hetero-tetramers with altered kinetic properties [3]. In a recent model LeBeau *et al.* required three control parameters (IP_3R phosphorylation and Ca^{2+} in- and efflux rates) to simulate the different patterns of Ca^{2+}-signaling evoked by CCK and acetylcholine in pancreatic acinar cell [15]. However, these authors did not consider the $c_{\rm ER}$ in their model. In our model a single control parameter $[IP_3]$ suffices for simulating CCK-induced Ca^{2+} signals. In the LeBeau model, the bifurcation diagram for CCK-induced model oscillations reveals that oscillations are present within a narrow range (0.55–0.75 μM) of $[IP_3]$. This implies that large changes in [CCK] result in small changes in $[IP_3]$. In our model, oscillations are initiated at a similar $[IP_3]$ but occur over a much broader range (0.6–6 μM) of IP_3. The latter is in agreement with the idea that each stimulus-receptor interaction event results in the formation of many second-messenger molecules. Within the oscillatory regime of our model, V_{IP_3} increases as a function of c and does not inactivate (data not shown). This is in line with experimental data obtained by Hagar *et al.* [17] for the type-III IP_3R (the major subtype in pancreatic acinar cells [18]). In our model, the oscillation interval is not determined by τ_h but by the filling state of the ER ($c_{\rm ER}$; data not shown). Therefore, the reduced filling state of the ER following IP_3-induced Ca^{2+} release is responsible for the period of insensitivity of the IP_3R for the prevailing $[IP_3]$. Only an elevation of $[IP_3]$ results in an increase of Ca^{2+} during the interspike interval. In this respect, our model perfectly simulates the phenomenon of "quantal" Ca^{2+} release originally described in [19].

In several tissues, Ca^{2+} has been proposed to function as an intercellular messenger traveling between cells through gap junctional diffusion (*e.g.*, [20]). In hepatocyte couplets [21] and

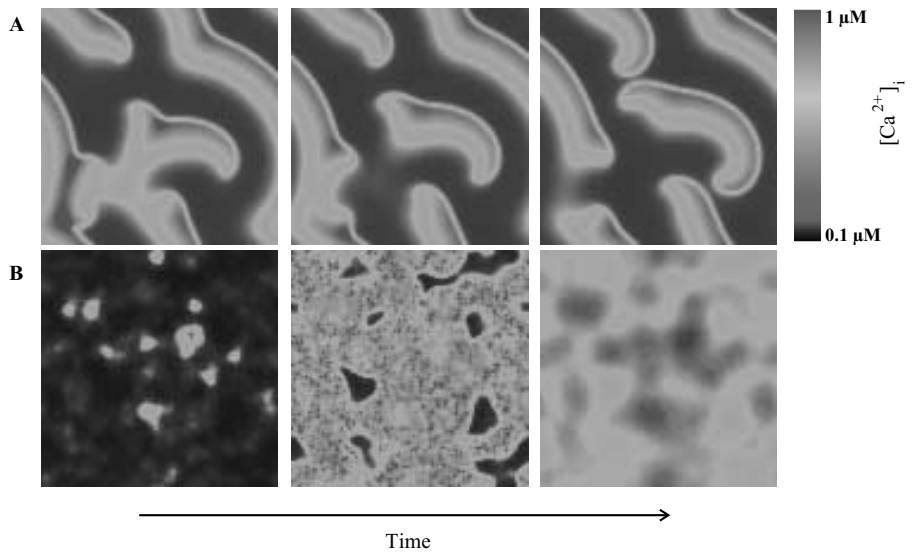

Fig. 5 – Spatio-temporal patterns occurring in a network with 100×100 units. Panel A (from left to right) shows several traveling waves characterized by partial synchronization of the Ca^{2+} release sites. Panel B (from left to right) shows an evolution of a coherent pattern in which the whole network was oscillating in phase. In both cases, the time interval between consecutive images was 5 s, $D_{\text{eff}}/\Delta^2 = 0.5\ \text{s}^{-1}$, $[\text{IP}_3] = 0.5\ \mu$M and $K_{\text{IP}_3}(\boldsymbol{x}) = (0.65 \pm 0.05)\ \mu$M. (For other parameters, see fig. 2.)

hippocampal slices [11] the presence of traveling and spiral Ca^{2+} waves has been described. Mechanistically, these regenerative waves are mediated by CICR that is triggered by diffusional Ca^{2+} entry from a neighboring cell [22]. To explore the possible use of our one-dimensional model for investigating such a mechanism, we built a regular $2d$ network with N units and a grid spacing Δ and assumed that the dynamics of each unit is driven by (1)-(4). To consider diffusion of Ca^{2+} we extended the right-hand side of eq. (1) with an additional diffusional term $D_{\text{eff}}\left(\frac{\partial^2 c(\boldsymbol{x},t)}{\partial x^2} + \frac{\partial^2 c(\boldsymbol{x},t)}{\partial y^2}\right)$, where $\boldsymbol{x} = (x, y)$ and D_{eff} is the diffusion constant. D_{eff} can be regarded as a term that extends the model with a description for Ca^{2+} diffusion through gap junctions. By studying its collective behavior, the presence of bistability and hysteresis in the network was investigated. This is important for validating future use of the model in the simulation of different types of Ca^{2+} waves. A useful magnitude to analyze the particular dynamics of the network is $\sigma_c^2 = \overline{(\langle c(\boldsymbol{x},t)\rangle - \langle c(\boldsymbol{x},t)\rangle)^2}$, where $\overline{f(t)} \equiv \frac{1}{T}\int_{t_0}^{t_0+T} f(t)\mathrm{d}t$, and $\langle\cdot\rangle$ is a spatial average over the whole network. This magnitude is a measure of the degree of temporal and spatial correlation in the activity between different regions in the network. In fig. 4A the dependence of σ_c with D_{eff}/Δ^2 (in units of s^{-1}) is shown for a square network of 60×60 units.

By slowly changing D_{eff}/Δ^2 a hysteresis loop in the collective dynamics of the network was revealed. The upper branch of the loop (relatively high σ_c) corresponds to a network with strong spatial correlations among Ca^{2+} release sites. This produces almost full synchronization between the release sites resulting in a coherent in-phase oscillation of the whole network without traveling waves (fig. 5B). The lower branch of the loop (relatively low σ_c) is associated to *partial synchronization* of the Ca^{2+} release sites. This results in emergence of quasi-periodic spatio-temporal patterns of synchronization like traveling waves and spirals moving along the network (fig. 5A). These patterns were recorded after a transient of 20000 s and remained stable during 2000 s with the only exception that the spatial position of the center of the

spirals changed in time. In fig. 4B we computed the phase diagram of this system. The figure shows the regions in the space of parameters (N, D_{eff}) where the different synchronization regimes appear. In all $2d$ simulations, we considered random initial conditions and periodic boundary conditions but the main observations were only marginally affected by the choice of these conditions. Also, we considered $[\text{IP}_3] = 0.5\ \mu\text{M}$ and K_{IP_3} to be a function of the position in the network taking random values around $0.65\ \mu\text{M}$, that is $K_{\text{IP}_3}(\boldsymbol{x}) = (0.65 \pm 0.05)\ \mu\text{M}$. This description assumes that the IP_3-sensitivity of each unit is not fully identical (which is reasonable given the biological variation between individual cells).

In conclusion, we introduced a mathematical model to explain Ca^{2+} oscillations in non-excitable cells (using pancreatic acinar cells as a biological model). The model features a detailed description of IP_3-mediated Ca^{2+} release and includes realistic assumptions about different fluxes described in real cells. Since the model faithfully reproduced experimental Ca^{2+} recordings, we analyzed the collective Ca^{2+} dynamics of a coupled $2d$ network of cellular models. Our findings stress the importance of the diffusion constant D_{eff} in the emergence of different spatio-temporal patterns of Ca^{2+} signaling in such a network. In the future we will use the $2d$ model to investigate traveling waves within single acinar cells. This will be achieved by considering each unit in the network as a spatial position within the cell and adjusting each parameter as a function of this position. After comparison with experimentally recorded Ca^{2+} waves, such a model enables investigation of the highly complex mechanistic aspects of spatio-temporal Ca^{2+} signals.

REFERENCES

[1] Berridge M. J., *Nature*, **361** (1993) 315.
[2] Putney J. W. jr., *Cell Calcium*, **7** (1986) 1.
[3] Miyakawa T., Maeda A., Yamazawa T., Hirose K., Kurosaki T. and Iino M., *EMBO J.*, **18** (1999) 1303.
[4] Goldbeter A., Dupont G. and Berridge M. J., *Proc. Natl. Acad. Sci. USA*, **87** (1990) 1461.
[5] Bezprozvanny I., Watras J. and Ehrlich B. E., *Nature*, **351** (1991) 751.
[6] Atri A., Amundson J., Clapham D. and Sneyd J., *Biophys. J.*, **65** (1993) 1727.
[7] Hofer A. M., Fasolato C. and Pozzan T., *J. Cell Biol.*, **140** (1998) 325.
[8] Petersen O. H., Burdakov D. and Tepikin A. V., *Bioessays*, **21** (1999) 851.
[9] Willems P. H. G. M., van Emst-de Vries S. E., van Os C.H. and de Pont J. J. H. H. M., *Cell Calcium*, **14** (1993) 145.
[10] Sneyd J., Keizer J. and Sanderson M. J., *FASEB J.*, **9** (1995) 1463.
[11] Wilkins M. and Sneyd J., *J. Theor. Biol.*, **191** (1998) 299.
[12] De Young G. W. and Keizer J., *Proc. Natl. Acad. Sci. USA*, **89** (1992) 9895.
[13] Sienaert I., Messiaen L., de Smedt H., Parys J. B., Sipma H. and Casteels R., *J. Biol. Chem.*, **272** (1997) 25899.
[14] Taylor C., *Biochim. Biophys. Act.*, **1436** (1998) 19.
[15] LeBeau A. P., Yule D. I., Groblewski G. E. and Sneyd J., *J. Gen. Physiol.*, **113** (1999) 851.
[16] Schutter E. D. and Smolen P., in *Methods in Neuronal Modeling*, edited by Koch C. and Segev I. (MIT Press, Cambridge, Mass.) 1999, p. 219.
[17] Hagar R. E., Burgstahler A. D., Nathanson M. H. and Ehrlich B. E., *Nature*, **396** (1998) 81.
[18] Wojcikiewicz R. J. and Luo S. G., *J. Biol. Chem.*, **273** (1995) 5670.
[19] Muallem S., Pandol S. J. and Beeker T. G., *J. Biol. Chem.*, **264** (1989) 205.
[20] Robb-Gaspers L. D. and Thomas A. P., *J. Biol. Chem.*, **270** (1995) 8102.
[21] Höfer T., *Biophys. J.*, **77** (1999) 1244.
[22] Höfer T., Politi A. and Heinrich R., *Biophys. J.*, **80** (2001) 75.